

## RESEARCH ARTICLE

10.1002/2014JB011408

## Key Points:

- We use 2-D thermomechanical models to study multiscale inversion tectonics
- Extensional inheritance facilitates the deformation of the overriding plate
- Basement deformation has a control on thin-skinned fold-and-thrust belts

## Supporting Information:

- Text S1
- Animation S1
- Animation S2
- Animation S3
- Animation S4
- Animation S5
- Animation S6

## Correspondence to:

Z. Erdős,  
zoltan.erdos@geo.uib.no

## Citation:

Erdős, Z., R. S. Huismans, P. van der Beek, and C. Thieulot (2014), Extensional inheritance and surface processes as controlling factors of mountain belt structure, *J. Geophys. Res. Solid Earth*, 119, 9042–9061, doi:10.1002/2014JB011408.

Received 25 JUN 2014

Accepted 23 OCT 2014

Accepted article online 28 OCT 2014

Published online 2 DEC 2014

## Extensional inheritance and surface processes as controlling factors of mountain belt structure

Zoltán Erdős<sup>1,2</sup>, Ritske S. Huismans<sup>1</sup>, Peter van der Beek<sup>2</sup>, and Cedric Thieulot<sup>1,3,4</sup>

<sup>1</sup>Department of Earth Sciences, University of Bergen, Bergen, Norway, <sup>2</sup>ISTerre, University Grenoble Alpes, Grenoble, France, <sup>3</sup>Now at Department of Earth Sciences, Utrecht University, Utrecht, Netherlands, <sup>4</sup>Now at Center for Earth Evolution and Dynamics, University of Oslo, Oslo, Norway

**Abstract** Surface processes and inherited structures are widely regarded as factors that strongly influence the evolution of mountain belts. The first-order effects of these parameters have been studied extensively throughout the last decades, but their relative importance remains notoriously difficult to assess and document. We use lithospheric scale plane-strain thermomechanical model experiments to study the effects of surface processes and extensional inheritance on the internal structure of contractional orogens and their foreland basins. Extensional inheritance is modeled explicitly by forward modeling the formation of a rift basin before reversing the velocity boundary conditions to model its inversion. Surface processes are modeled through the combination of a simple sedimentation algorithm, where all negative topography is filled up to a prescribed reference level, and an elevation-dependent erosion model. Our results show that (1) extensional inheritance facilitates the propagation of basement deformation in the retro-wedge and (2) increases the width of the orogen; (3) sedimentation increases the length scale of both thin-skinned and thick-skinned thrust sheets and (4) results in a wider orogen; (5) erosion helps to localize deformation resulting in a narrower orogen and a less well-developed retro-wedge. A comparison of the modeled behaviors to the High Atlas, the Pyrenees, and the Central Alps, three extensively studied natural examples characterized by different degrees of inversion, is presented and confirms the predicted controls of surface processes and extensional inheritance on orogenic structure.

### 1. Introduction

The crustal structure of collisional orogens around the world shows a wide range of deformation styles from narrow, asymmetric doubly vergent wedges like the Pyrenees [Muñoz, 1992] to wide, plateau-like orogens such as the Zagros mountain belt in Iran [Mouthereau *et al.*, 2007]. Recently, Jamieson and Beaumont [2013] proposed a conceptual temperature-magnitude framework for orogenesis in terms of the progression from small-cold to large-hot orogens. In the proposed framework, small-cold orogens are defined to be those in which the upper part of the lithospheric mantle subducts with little internal deformation and bulk shortening and where crustal thickening and heating are limited. In contrast, large-hot orogens are typically composed of a central elevated plateau underlain by thick crust and underthrust continental lithosphere and characterized by major internal deformation, strong heating and ductile flow of the middle lower crust.

In this framework, the most important controlling factor on the size and overall structure of an orogen is the amount of convergence between the colliding plates. However, in addition to the amount of convergence, several other factors have been proposed to provide a first-order control on the structural development of mountain belts, including bulk crustal strength, inherited weaknesses, and the efficiency of surface process. While these parameters have been studied extensively in the last decades [e.g., Beaumont *et al.*, 1992; Willett *et al.*, 1993; Mugnier *et al.*, 1997; Stolar *et al.*, 2006; Buiter, 2012; Jammes and Huismans, 2012; Mouthereau *et al.*, 2013], questions still remain about their exact effects on the style of orogenic development.

Numerous studies have shown that the strength of the crust and the mantle lithosphere provide first-order controls on the structural style in both extensional [Buck, 1991; Bassi *et al.*, 1993; Buck *et al.*, 1999; Huismans and Beaumont, 2003, 2011; Huismans *et al.*, 2005; Jammes and Huismans, 2012] and contractional [Willett *et al.*, 1993; Beaumont *et al.*, 1994; Ellis *et al.*, 1998; Jammes and Huismans, 2012] settings. In addition, as Jammes and Huismans [2012] pointed out most recently, the strength of the crust is highly dependent on inherited compositional and structural weaknesses. Although most orogens initiate by inversion of passive margins or rifted basins, little is known about how inherited extensional

structures affect the evolution of these orogens. Previous studies focused mainly on the effect of inheritance on the scale of half-graben systems [Buiter and Pfiffner, 2003] and moderate inversion of rifted basins exploring the effects of postrift thermal equilibration [Buiter et al., 2009]. Jammes and Huismans [2012] demonstrated that rifting inheritance can explain the presence of a lower crustal or mantle lithospheric body at shallow depth, as inferred for the Pyrenees [Muñoz, 1992] and European Alps [Schmid and Kissling, 2000], for example. Extensional inheritance also appears to facilitate the propagation of deformation to the retro-wedge of the orogen [Jammes and Huismans, 2012]. However, their modeling study focused mainly on the thick-skinned crustal-scale evolution of mountain belts, the numerical model resolution being insufficient to properly address the link with thin-skinned structures and processes acting at the Earth's surface.

The effects of erosional processes on the tectonic evolution of mountain belts have been extensively studied [see Whipple, 2009, and references therein], and it has been shown that erosion is not only a response to topographic growth resulting from mountain building but that it has potentially strong feedbacks on the development of the internal structure of orogens [e.g., Beaumont et al., 1992; Avouac and Burov, 1996; Willett, 1999]. It has also been shown that syntectonic sedimentation has a strong control on the structure of thin-skinned fold-and-thrust belts [e.g., Storti and McClay, 1995; Ford, 2004; Simpson, 2006; Bonnet et al., 2007; Fillon et al., 2012], where the erosion products from the orogenic hinterland can stabilize the belt in accordance with critical-taper theory [Chapple, 1978; Dahlen, 1990]. However, despite our improved understanding of the control exerted by surface processes on the evolution of contractional orogens, it is still unclear how they might affect mountain building in the presence of inherited extensional structures. Neither has much work been done to decipher which aspects of orogenic structure and evolution can be ascribed to tectonic inheritance or to surface processes specifically, and which of these provide the prime control on the structure of individual mountain belts.

Here we study the effect of inherited extensional structures and surface processes on the deformation style of collisional orogens as well as their adjacent foreland fold-and-thrust belts. Moreover, the interaction of thin-skinned and thick-skinned tectonics is explored with the use of a shallow frictionally weak detachment at the base of a predeformation sedimentary layer. We investigate the effects of extensional inheritance by modeling the formation of a continental rift basin explicitly before the velocity boundary conditions are inverted to create a contractional environment for the development of a doubly vergent orogen. In this “accordion” modeling approach (using the term coined by Jammes and Huismans [2012]) the structure predicted by an extensional model is used as the initial conditions for modeling inversion tectonics. The effects of sedimentation are included using a simple model where the topography is filled up with sediments to a reference level, while erosion is modeled with an elevation-dependent algorithm. A first-order comparison of our model results with natural examples from the High Atlas, the Pyrenees, and the European Alps suggests that our model experiments can be used to explain characteristic features of these and other natural systems.

## 2. Methodology

### 2.1. Basic Principles

We use a modified version of the Arbitrary Lagrangian-Eulerian finite-element code FANTOM to solve the Stokes and the heat transport equations [Thieulot, 2011]. We model thermo-mechanically coupled, plane-strain, incompressible viscous-plastic creeping flows to investigate the behavior of a layered lithosphere with frictional-plastic and thermally activated power law viscous rheologies in both extensional and contractional regimes. When stress is below the frictional-plastic yield criterion, deformation is viscous; frictional-plastic deformation is activated when the stress exceeds the yield criterion. The numerical accuracy of the finite-element code has been verified through benchmarking against a wide range of analytical and numerical studies [Thieulot, 2011].

Viscous flow follows temperature-dependent nonlinear power law rheologies. The effective viscosity  $\eta_{\text{eff}}$  is specified as

$$\eta_{\text{eff}} = f \cdot A^{-1/n} \cdot \dot{\epsilon}^{(1-n)/2n} \cdot \exp\left(\frac{Q + V \cdot p}{nRT}\right) \quad (1)$$

**Table 1.** Mechanical and Thermal Parameters Used in the Thermomechanical Model Experiments<sup>a</sup>

Parameter (Units)	Salt	Upper Crust/Precollision Sediment	Lower Crust	Mantle Lithosphere	Sublithospheric Mantle
<i>Mechanical Parameters</i>					
Thickness (km)	1	21; 3	10	85	480
Reference density (kg m <sup>-3</sup> )	2300	2800	2800	3360	3300
Internal friction angle $\phi_{\text{eff}} (\epsilon)$	2°	15°–2°	15°–2°	15°–2°	15°–2°
Strain range of softening	-	0.5–1.5	0.5–1.5	0.5–1.5	0.5–1.5
Cohesion (Pa)	-	$2 \cdot 10^7$ – $4 \cdot 10^6$	$2 \cdot 10^7$ – $4 \cdot 10^6$	$2 \cdot 10^7$ – $4 \cdot 10^6$	$2 \cdot 10^7$ – $4 \cdot 10^6$
Flow law	-	Wet Quartz		Dry Olivine	
scaling factor ( <i>f</i> )	-	1	100	1	1
<i>A</i> (Pa <sup>-<i>n</i></sup> s <sup>-1</sup> )	-	$8.574 \cdot 10^{-28}$	$8.574 \cdot 10^{-28}$	$2.4168 \cdot 10^{-15}$	$1.393 \cdot 10^{-14}$
<i>Q</i> (J mol <sup>-1</sup> )	-	$222.81 \cdot 10^3$	$222.81 \cdot 10^3$	$540.41 \cdot 10^3$	$429.83 \cdot 10^3$
<i>n</i>	-	4	4	3.5	3
<i>V</i> (m <sup>3</sup> mol <sup>-1</sup> )	-	$3.1 \cdot 10^{-6}$	$3.1 \cdot 10^{-6}$	$25 \cdot 10^{-6}$	$15 \cdot 10^{-6}$
<i>R</i> (J mol <sup>-1</sup> °C <sup>-1</sup> )	-	8.3144			
<i>Thermal Parameters</i>					
Thermal diffusivity (m <sup>2</sup> s <sup>-1</sup> )	$1 \cdot 10^{-6}$	$1 \cdot 10^{-6}$	$1 \cdot 10^{-6}$	$1 \cdot 10^{-6}$	$1 \cdot 10^{-6}$
Thermal expansion (K <sup>-1</sup> )	$3.1 \cdot 10^{-5}$	$3.1 \cdot 10^{-5}$	$3.1 \cdot 10^{-5}$	0	0
Heat productivity (W m <sup>-3</sup> )	$0.8 \cdot 10^{-6}$	$0.8 \cdot 10^{-6}$	$0.8 \cdot 10^{-6}$	0	0

<sup>a</sup>We note that due to direct matrix solver limitations the maximum effective viscosity difference that can be resolved is 9 orders of magnitude; hence, we use cut off values of  $\eta_{\text{eff}}^{\text{min}} = 10^{20}$  and  $\eta_{\text{eff}}^{\text{max}} = 10^{28}$  Pa s.

where *A* is the preexponential scaling factor, *n* is the power law exponent,  $\epsilon$  is the second invariant of the deviatoric strain rate tensor ( $\frac{1}{2} \dot{\epsilon}'_{ij} \dot{\epsilon}'_{ij}$ ), *Q* is activation energy, *V* is activation volume, *p* is pressure, *T* is temperature, and *R* is the universal gas constant. *A*, *n*, *Q*, and *V* are derived from laboratory measurements carried out on “wet” and “dry” olivine and “wet” quartzite [Karato and Wu, 1993; Gleason and Tullis, 1995] and are given in Table 1. A factor *f* is chosen to scale viscosities calculated from the reference wet quartzite flow law for the lower crust. The effective viscosity of the crust remains largely unconstrained [Huismans and Beaumont, 2003]; the applied viscosity scaling represents a simple technique that can be used to create strong lower crust without recourse to additional flow laws that are subject to significant uncertainties.

Frictional-plastic yielding is modeled with a pressure-dependent Drucker-Prager yield criterion, equivalent to the Coulomb yield criterion, when modeling incompressible deformation in plane strain. Yielding occurs when

$$(\dot{J}'_2)^{1/2} = p \cdot \sin(\phi_{\text{eff}}) + C \cdot \cos(\phi_{\text{eff}}) \quad (2)$$

where  $\dot{J}'_2$  is the second invariant of the deviatoric stress,  $\phi_{\text{eff}}$  is the effective internal angle of friction given as  $p \cdot \sin(\phi_{\text{eff}}) = (p - p_f) \cdot \sin(\phi)$  for pore-fluid pressure *p<sub>f</sub>*, and cohesion *C*. With appropriate choice of cohesion and effective internal angle of friction [e.g., Lavier et al., 2000], this yield criterion can approximate the effect of pore-fluid pressure and frictional sliding in rocks. High transient or static fluid pressures or mineral transformations can cause the weakening of frictional-plastic faults and shear zones [Sibson, 1990; Streit, 1997; Bos and Spiers, 2002]. In the model, these strain-softening effects are accounted for through a linear decrease of the effective internal angle of friction from 15° to 2°, with a simultaneous decrease of the cohesion from 20 MPa to 4 MPa for accumulated strain values between 0.5 and 1.5 (Figure 1b). We note that  $\phi_{\text{eff}} (\epsilon) \approx 15^\circ$  corresponds to the effective internal angle of friction when the pore-fluid pressure is approximately hydrostatic. Note that strain-healing mechanisms have not been accounted for in these models.

In addition to solving the Stokes equation for viscous-plastic flows, the heat transport equation is solved in two dimensions (*i* = 1, 2):

$$\rho \cdot C_p \cdot \left( \frac{\partial T}{\partial t} + v_i \frac{\partial T}{\partial x_i} \right) = \frac{\partial}{\partial x_i} \cdot \left( k \frac{\partial T}{\partial x_i} \right) + H \quad (3)$$

where  $\rho$  is density, *C<sub>p</sub>* is heat capacity, *t* is time, *v<sub>i</sub>* and *x<sub>i</sub>* are the velocity and spatial components in the *i* direction, *k* is thermal conductivity, and *H* is heat production per unit volume. The mechanical and thermal

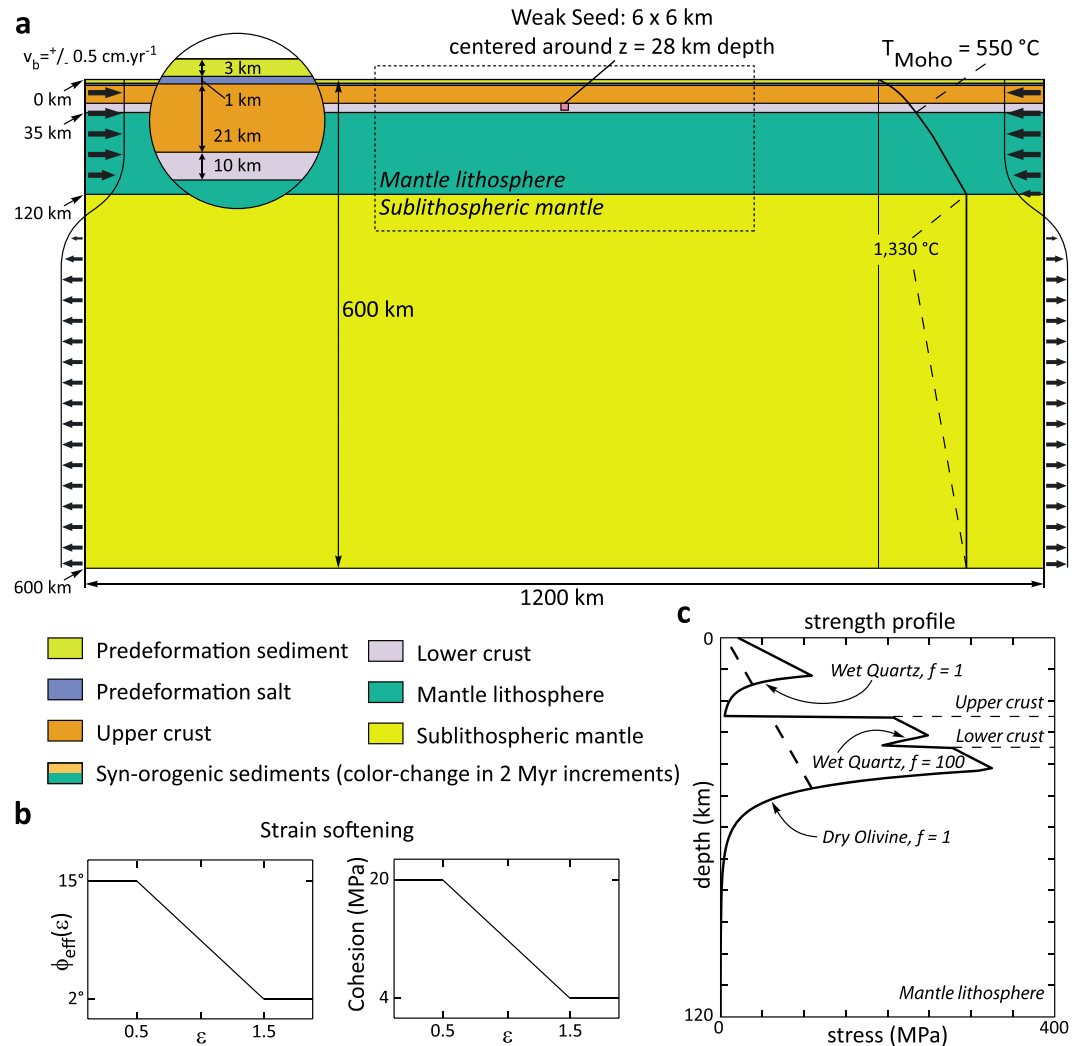


**Figure 1.** (a) Model geometry showing layer thicknesses, the position and size of the weak seed, the lateral velocity boundary conditions, and the initial temperature profile. All values used for the mechanical and thermal parameters are listed in Table 1. The lateral velocity boundary condition is set up to achieve mass balance. Extension and contraction are driven by the velocity boundary conditions and seeded by a small strain-weakened region. The dotted rectangle demonstrates the size of the excerpts shown in Figures 2–8. (b) Frictional-plastic strain softening is achieved through a linear decrease of  $\phi_{\text{eff}}$  from 15° to 2° with a simultaneous decrease of  $C$  from 20 MPa to 4 MPa. (c) The initial strength profiles of the models. The dashed line represents the fully strain-weakened state of the lithosphere.

systems are coupled through the temperature-dependent rheologies and are solved sequentially for each model time step. The temperature dependence of the densities is given by

$$\rho(T) = \rho_0(1 - \alpha(T - T_0)) \quad (4)$$

with the thermal expansion coefficient  $\alpha = 3.1 \cdot 10^{-5} \text{ }^\circ\text{C}^{-1}$  for the crust and  $\alpha = 0^\circ\text{C}^{-1}$  for the mantle. The reference densities of the individual materials at  $T_0 = 0^\circ\text{C}$  are given in Table 1. A compositional density contrast of  $60 \text{ kg m}^{-3}$  between the mantle lithosphere and sublithospheric mantle is applied in order to avoid small-scale mantle-flow instabilities.

## 2.2. Model Setup

The models are set up as an idealized representation of the lithosphere and the sublithospheric mantle in a 600 km high and 1200 km wide box (Figure 1a). The lithosphere consists of a 35 km thick crust (25 km upper crust, 10 km lower crust) and 85 km mantle lithosphere overlying the sublithospheric mantle. The top

**Table 2.** List of Model Experiments and Their Varying Parameters

Model	Amount of Extension	Sedimentation (Start)	Erosion Rate	Figure
M1 (reference)	50 km	-	-	Figure 2
M2	-	-	-	Figure 4
M3	100 km	-	-	Figure 5
M4	50 km	20 Myr	-	Figure 6
M5	50 km	20 Myr	$4.35 \cdot 10^{-15} \text{ s}^{-1}$	Figure 7
M6	50 km	20 Myr	$8.7 \cdot 10^{-15} \text{ s}^{-1}$	Figure 8

4 km of the crust represent prerift sediments composed of a 3 km thick frictional upper layer overlying a 1 km thick weak layer representing a décollement level (e.g., salt). This setup allows for modeling the behavior of prerift sedimentary sequences as well as the deformation of the underlying continental basement, providing insight into the potential coupling and interaction of thin-skinned and thick-skinned tectonic regimes.

To ensure that the deformation localizes in the center of the model rather than at the sides, where boundary effects may influence the deformation pattern, we initially place a strain-weakened rectangular seed of 6 by 6 km positioned at the top of the strong, frictional-plastic lower crust. Also note that since the initial conditions are symmetrical, subduction initiates with a random polarity for each model. For ease of comparison, we have reoriented some of the models so they all show the same polarity.

The Eulerian grid consists of 2400 elements in the horizontal and 300 elements in the vertical dimension, respectively. The distribution of the elements is irregular in the vertical direction, with 125 elements in the upper crust, 125 elements in the lower crust and mantle lithosphere, and 50 elements in the sublithospheric mantle. Consequently, the resolution in the horizontal direction is equal to 500 m for the entire model domain, while the vertical resolution is 200 m in the upper crust, 800 m in the lower crust and mantle lithosphere, and 9.5 km in the sublithospheric mantle. Initially, each cell of the Eulerian grid contains nine Lagrangian (material) nodes that allow for the tracking of the materials through space and time. Additionally, a third grid is defined and tracked purely for visualization purposes.

A free surface at the top of the numerical model allows for tracking directly the evolution of the topography, with minimal surface smoothing applied in a controlled manner, to prevent numerical instabilities. Velocity boundary conditions are imposed on both vertical sides of the model while a free slip condition is applied at its base. In extensional mode, material is flowing out through both sidewalls of the model in the lithosphere with a velocity  $v = 0.5 \text{ cm/yr}$ , while material is flowing in through both sidewalls in the sublithospheric mantle with a velocity scaled to balance the outflow of lithospheric material (Figure 1a). In convergence mode, the lateral boundary conditions are inverted. We have not explored the effects of varying extension and contraction velocities and note that postrift thermal relaxation is not accounted for.

The lateral boundaries are thermally insulated (i.e., heat flow is not allowed through the boundary), while the top and basal boundaries are set to a constant temperature (Figure 1a). The initial temperature field is laterally uniform and increases parabolically with depth from the surface ( $T_0 = 0^\circ\text{C}$ ) to the base of the crust (initial Moho temperature,  $T_m = 550^\circ\text{C}$ ) as a result of heat production in the crust ( $h_c = 0.8 \mu\text{Wm}^{-3}$ ). Below the Moho, temperature follows a linear gradient to the base of mantle lithosphere (initially at  $T = 1330^\circ\text{C}$ ); the temperature of the sublithospheric mantle is initially constant and uniform.

The numerical models have a depth-dependent rheology in which the crust is characterized by the viscous creep parameters for wet quartz [Gleason and Tullis, 1995]. A scaling factor  $f_c = 100$  is used to obtain a strong lower crust. The mantle lithosphere is characterized by the viscous flow parameters of dry olivine [Karato and Wu, 1993], while the sublithospheric mantle is characterized by viscous flow parameters for wet olivine [Karato and Wu, 1993]. Using these parameters in the reference model, the upper crust (including the precollision sediments), the upper part of the strong lower crust and the top of the mantle lithosphere undergo frictional-plastic deformation, while the middle crust, the lower part of the lower crust, and the lower mantle lithosphere and sublithospheric mantle deform viscously (Figure 1c).

### 2.3. Surface Processes

The reference model (Model M1) does not account for sedimentation and erosion. The top of the model is acting as a free surface with only minimal surface smoothing applied to prevent numerical instabilities (see previous section).

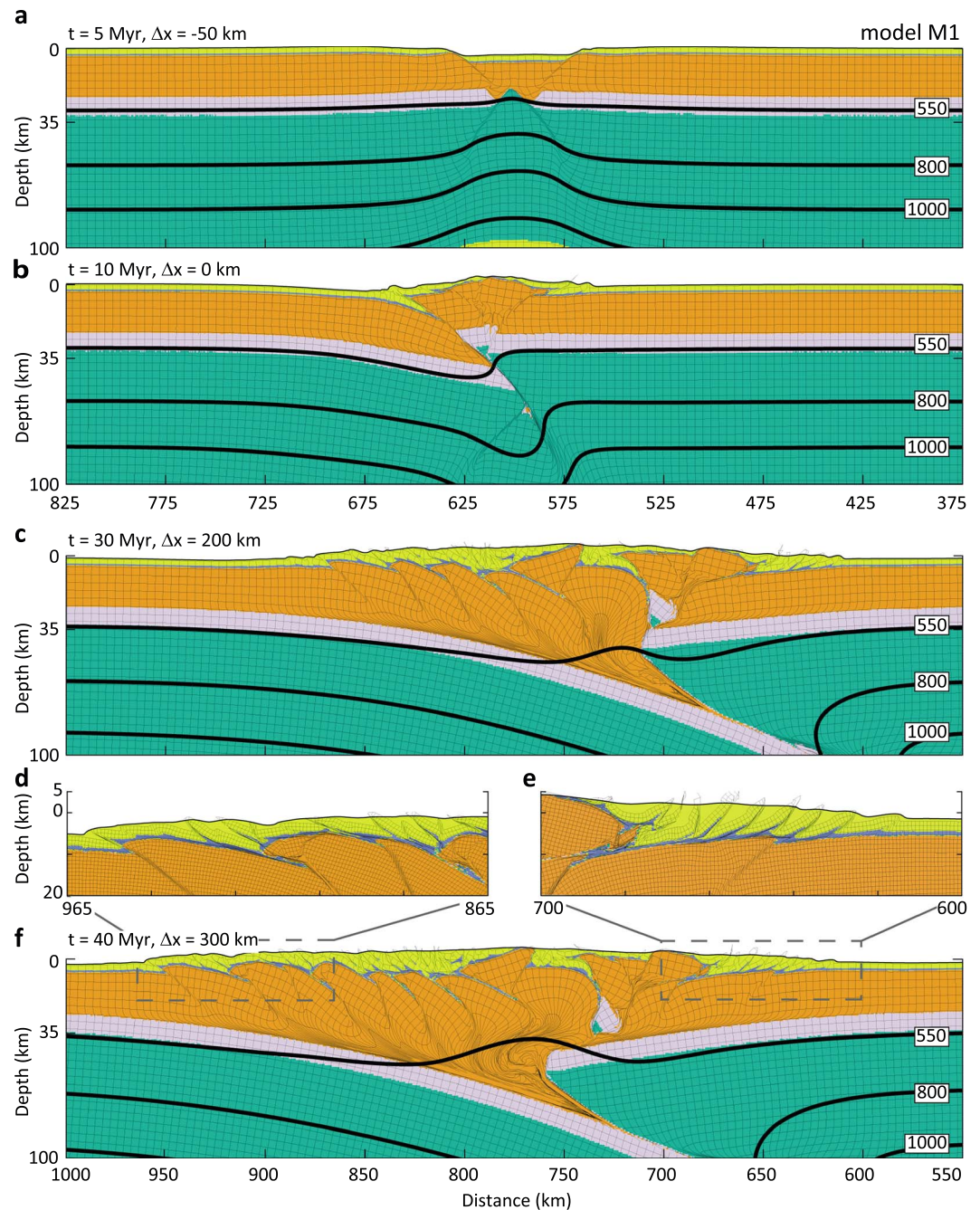


**Figure 2.** Reference model (M1) with no surface processes, showing deformed Lagrangian mesh and sample isotherms after (a) 5 Myr ( $\Delta x = -50$  km) extension, (b) 10 Myr ( $\Delta x = 0$  km) full inversion, (c) 30 Myr ( $\Delta x = 200$  km) contraction, and (f) 40 Myr ( $\Delta x = 300$  km) contraction for dashed area in Figure 1. (d and e) Zoomed extracts from Figure 2f to show the small-scale deformation patterns in the foreland fold-and-thrust belts. (Animations of model evolutions can be found in the online supporting information.)

In models M2–M4, a simple sedimentation model is applied. Deposition starts after 100 km of crustal shortening has taken place beyond full inversion and is modeled by filling all topography below a reference level with sediments at the end of each time step. The delayed initiation of sedimentation allows for the development of a more than 2 km high orogenic core that could provide a source for the sediments. This representation of sedimentation is very simple but the resulting geometry of the basin fill

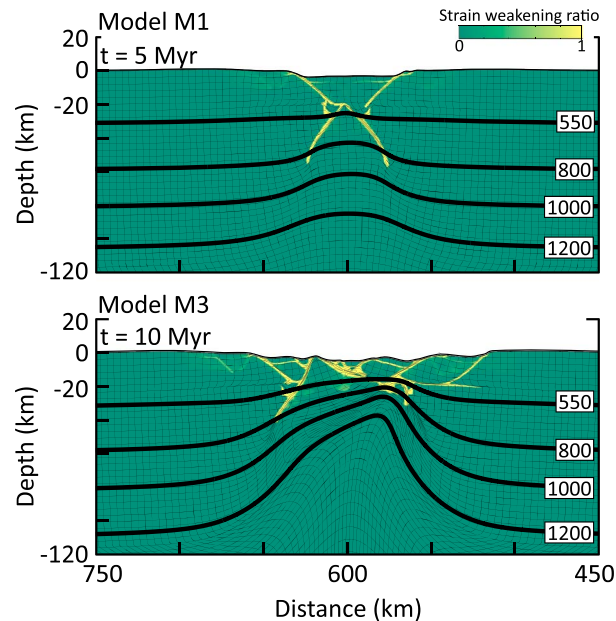


**Figure 3.** The spatial distribution of strain-weakening values on a scale of 0 to 1, where 0 (green) represents no strain weakening and 1 (yellow) represents full strain-weakening for models M1 and M3. The sections present the state of the crust at the end of the extensional phase for (a) model M1 (5 Myr and  $\Delta x = -50$  km) and (b) model M3 (10 Myr and  $\Delta x = -100$  km).

is consistent with natural foreland basin systems [DeCelles and Giles, 1996]. The deposited sediments have the same material properties as the upper crust and the precollision sediments.

In models M5 and M6, an elevation-dependent erosion algorithm is implemented following the equation  $\Delta h/\Delta t = h \cdot E_r$ , where  $h$  is elevation,  $\Delta t$  is time (s), and  $E_r$  is the characteristic inverse erosional timescale ( $s^{-1}$ ).  $E_r$  is scaled such that in model M3 a 4 km high topography erodes by 1 km in 2 Myr (later referred to as “moderate erosion rate”), while in model M4 this will take place in 1 Myr (later referred to as “high erosion rate”). The erosion algorithm used here is deliberately simple as it is intended for modeling the first-order effects of erosion without having to implement computationally demanding process-based algorithms [e.g., Stolar *et al.*, 2006].

Note that the two surface-process algorithms are not mass conserving, a simplification that allows for the separate

testing of the effects of sedimentation and erosion. Nevertheless, material that was initially deposited in the model can be eroded when elevated above the reference base level (fixed to the top left node of the model).

### 3. Results

A list of all models presented and their key parameters is provided in Table 2. Following the reference model (model M1; Figure 2), a set of models is presented that investigates the effect of varying the amount of initial extension on the orogens after inversion and contraction (models M2 and M3; Figures 4 and 5). Subsequently, the effects of surface processes (erosion/deposition) on the evolution of an orogen formed by inversion of a rift basin are explored (models M4 to M6; Figures 6–8).

#### 3.1. Reference Model: Model M1

The reference model starts in extensional mode with 50 km extension applied in 5 Myr before the velocity boundary conditions are reversed, creating contraction for the rest of the model experiment. The reference model has a weak decoupling horizon in the middle crust and a strong lower crust, with crustal scaling factors  $f_{uc} = 1$  and  $f_{lc} = 100$ . Neither sedimentation nor erosion is allowed for during the experiment. The model run can be divided into four phases that each display fundamentally different behavior (Figure 2). During Phase 1, extension leads to the formation of a largely symmetric continental rift basin bounded by two well-defined frictional-plastic normal shear zones. By the end of this phase (at  $t = 5$  Myr and 50 km extension) the strong lower crust is ruptured (Figure 2a), the rift basin is about 4 km deep at its deepest point, while the rift shoulders reach up to 1 km above the reference level. The prerift sediments display very little deformation. The relative degree of strain weakening (varying between 0 and 1) is used to visualize the distribution of frictional-plastic strain-weakened areas at the end of extension that provide the inherited structures for inversion (e.g., Figure 3). At the end of the extensional phase, strain weakening has occurred on highly discrete extensional shear zones in the upper crust and within the mantle lithosphere that will provide the inherited weak zones for the contraction phase (Figure 3a).

Phase 2 starts with the inversion of the velocity boundary conditions. By  $t = 10$  Myr (after 50 km contraction, equal to the amount of initial extension), the extensional basin is fully inverted. A mildly asymmetric

keystone structure with a lower crustal/mantle-lithospheric root is uplifted along the inverted frictional-plastic shear zones (Figure 2b). At this point, one of the inherited frictional-plastic shear zones is preferred over the other, leading to the initiation of continental subduction. The prerift sediment layer on top of the keystone structure gradually thins out as material slides down along the décollement layer toward the foredeep depressions on either side of the keystone block. At the same time, the first thin-skinned thrust sheets form in the footwall of the uplifted central block.

During Phase 3, deformation migrates into the subducting plate and starts building up the pro-wedge as a result of the continuing contraction (note that we use the terms pro-wedge and retro-wedge to define the deformed parts of the lower and upper plate, respectively, as defined by *Ellis et al.* [1998]). An outward propagating sequence of basement thrust sheets forms (Figure 2c) with thin-skinned deformation focused in the footwall of the active basement thrusts throughout the entire model experiment (see also Figures 2d and 2e). The sequence is only disrupted by the formation of a crustal-scale pop-up structure early on in its development, after abandonment of the first basement thrust sheet. The initial keystone structure that makes up the bulk of the retro-wedge is slowly translated along the inverted normal fault bounding the overriding plate, with thin-skinned deformation occurring in the footwall of the basement fault above the shallow décollement. The overriding plate itself remains relatively undeformed until 30 Myr.

During the final phase, pro-wedge deformation continues while the entire mass of the initial keystone structure, including its lower crustal root, is thrust onto the overriding plate, bending it gently down toward the subduction zone. Deformation penetrates the previously undeformed basement of the overriding plate and two thick-skinned thrust sheets form, widening the retro-wedge significantly (Figure 2f). The displacement along the individual basement thrusts in the retro-wedge is notably less than in the pro-wedge.

### 3.2. Model Sensitivity to the Amount of Extension: Models M2 and M3

Models M2 and M3 test the effect of the amount of extension on the structural style of lithospheric inversion. In model M2, the effect of extensional inheritance is removed by running the model in contractional mode only (model M2; Figure 4). In model M3, in contrast, the extensional mode is run until full crustal breakup before inverting the velocity boundary conditions (model M3; Figure 5). Neither sedimentation nor erosion is allowed for in these experiments. These two models investigate end member values in terms of initial crustal extension (zero versus full crustal breakup).

#### 3.2.1. Pure Contraction: Model M2

The effects of extensional inheritance on mountain building can be understood best in comparison to a purely contractional model. In the absence of extension, the development of model M2 (Figure 4) can be divided into two phases. During Phase 1, shortening results in the uplift of a symmetrical keystone structure, narrower than in the reference model with extension, with foreland depressions developing on either side. The keystone structure incorporates very little lower crustal material and no mantle lithosphere at all. Continental subduction is initiated as soon as deformation localizes preferentially on one of the shear zones bounding the keystone structure, accommodating shortening within the strong lower crust and mantle lithosphere. The small lower crustal root of the keystone structure remains close to the top of the undeformed lower crust of the overriding plate throughout the model experiment. With continued crustal shortening, thin-skinned thrust sheets form in the footwall of the keystone structure, detaching in the décollement layer at the base of the preorogenic sediments, while deformation in the crust propagates toward the foreland in the subducting plate with the formation of a basement thrust sheet (Figure 4a).

Subsequently, shortening is accommodated in turn by the formation of new basement thrust sheets propagating to the foreland, and by the formation of thin-skinned thrusts in the precollision sediments in the footwall of the active basement thrust sheet (Figures 4b–4d). The overriding plate remains relatively undeformed throughout the model evolution, developing a single basement thrust sheet and only limited thin-skinned deformation after 300 km of contraction (Figures 4c and 4d).

#### 3.2.2. Full Breakup: Model M3

In model M3, 100 km of initial extension results in full crustal breakup (Figure 5a). The model experiment can be divided into four phases (Figures 5a–5f). During the first phase, early rupture of the strong lower crust is followed by the formation of a wide, asymmetric rift basin with three rotated upper crustal fault blocks that are situated directly on top of the extended mantle lithosphere. The strain-weakening plot reveals that a fourth extensional shear zone is in the process of being activated (Figure 3b). This phase ends with full



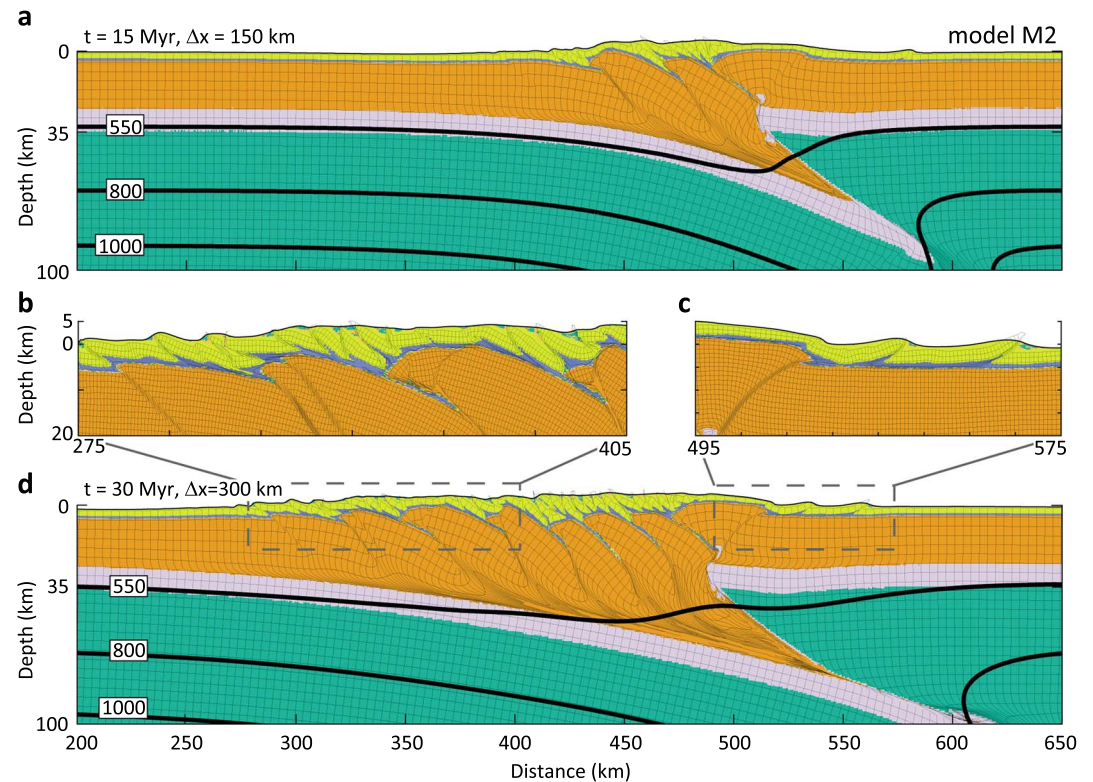


**Figure 4.** Pure contractional model M2 after (a) 15 Myr ( $\Delta x = 150$  km) contraction and (d) 30 Myr ( $\Delta x = 300$  km) contraction respectively; (b and c) zoomed extracts from Figure 4d to show the small-scale deformation patterns in the foreland fold-and-thrust belts. Sedimentation and erosion are not accounted for. The small pockets of syntectonic sediments present in the model are artifacts resulting from the surface smoothing.

crustal breakup after 10 Myr and 100 km of extension, leading to exhumation of mantle lithosphere (Figure 5a). The rift basin is about 5 km deep at its deepest point, while the rift flanks reach elevations up to 1.5 km. The prerift sediments display only minor deformation as they slide off from the tilted corners of the rotated fault blocks. No significant thin-skinned fault activity is apparent at this stage.

Phase 2 starts at the onset of inversion. During this phase, which lasts until 20 Myr, inversion of the preexisting extensional structures leads to a wider and more complex asymmetric keystone structure, which is uplifted along the most external inverted normal faults. Several smaller inversion structures develop in between these master faults, reflecting the complex structure of the rift basin (Figure 5b). The keystone structure involves only a marginally larger amount of lower crust and mantle lithosphere at its root, in comparison with the reference model that experienced less extension (Figure 2b). Thin-skinned deformation of the prerift sediments is minimal at this stage, with a few thrusts developing in the footwalls of the inverted extensional structures.

Phase 3 of the model evolution and onward is very similar to that of the reference model (Figures 5c and 5d). Deformation migrates into the subducting plate, building up the pro-wedge through an outward propagating sequence of basement thrust sheets. This sequence is again temporarily interrupted by the formation of a crustal-scale pop-up structure (Figure 5c; compare to Figure 2c). Thin-skinned deformation in the pro-wedge is concentrated in the footwall of the active basement thrusts. The keystone structure forming the retro-wedge is progressively transported along the inverted normal fault bounding the overriding plate, with minor thin-skinned deformation in the footwall of the basement fault above the shallow décollement. During the final phase, the keystone structure and adjacent thick-skinned basement thrusts are transported onto the overriding plate, bending it down toward the subduction zone. At this stage, after slightly more convergence than in the case of the reference model, a new thick-skinned thrust forms in the previously undeformed basement of the overriding plate (Figure 5f). The displacement along the individual basement thrusts in the retro-wedge is notably less than in the pro-wedge.

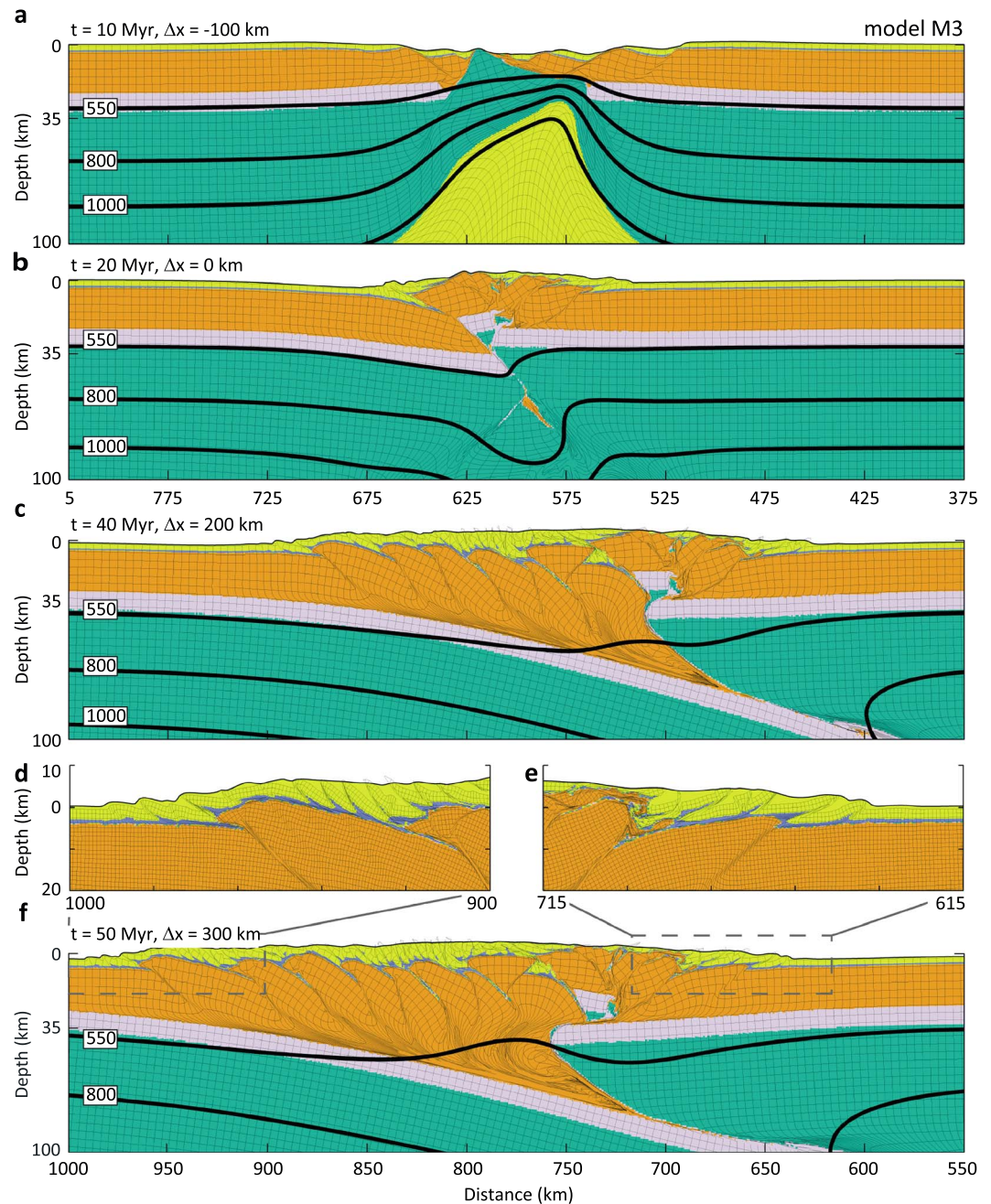


**Figure 5.** Model M3 undergoes extension until full crustal breakup before activating the inversion mode. Sedimentation and erosion are not accounted for. Presenting the same model properties as in the reference model (Figure 2) after (a) 10 Myr ( $\Delta x = -100$  km) extension, (b) 20 Myr ( $\Delta x = 0$  km) after full inversion, (c) 40 Myr ( $\Delta x = 200$  km) contraction, and (f) 50 Myr ( $\Delta x = 300$  km) contraction, respectively. (d and e) Zoomed extracts from Figure 5f to show the small-scale deformation patterns in the foreland fold-and-thrust belts.

### 3.3. The Effect of Sedimentation: Model M4

Model M4 has the same rheological setup as the reference model, with decoupling in the middle crust, a scaling factor  $f_{uc} = 1$  for the upper crust and  $f_{lc} = 100$  for the lower crust (Figure 6). Sedimentation is included, while erosion is not accounted for in this model. The experiment can be divided into four different phases, similar to the reference model. As sedimentation is only initiated after full inversion, the first two phases are identical to those of the reference model, with formation of a symmetric rift basin during

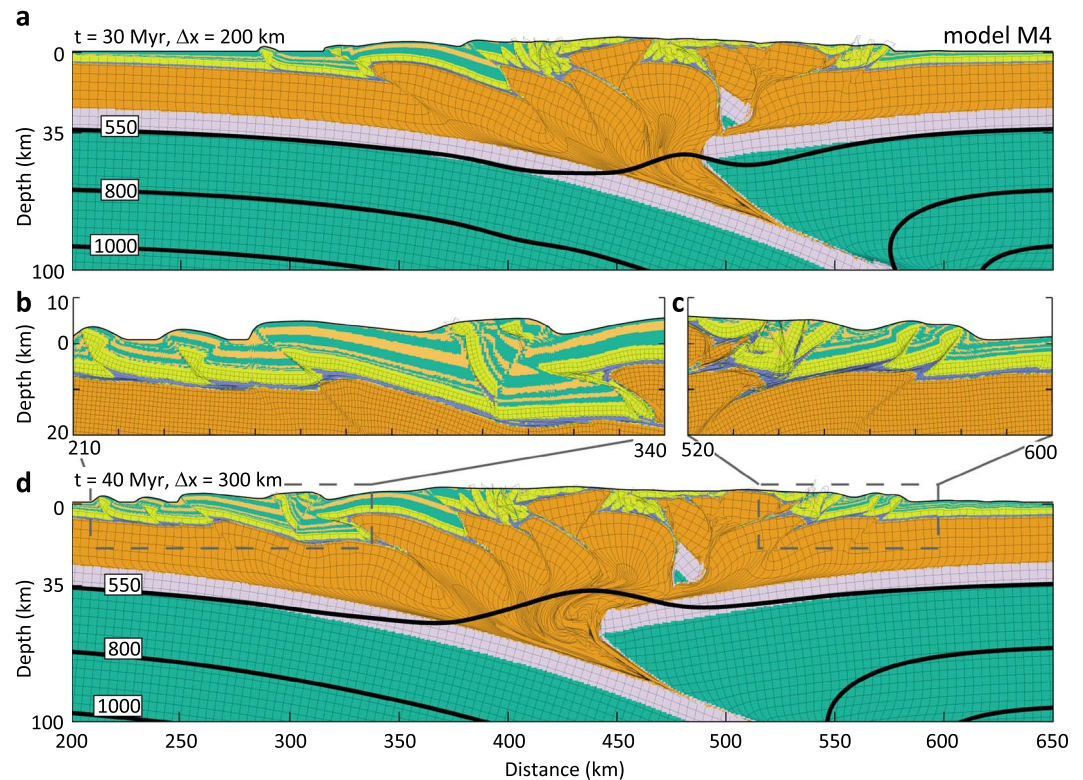


**Figure 6.** Model M4 including a simple sedimentation model. Presenting the same model properties as in the reference model (Figure 2) after (a) 30 Myr ( $\Delta x = 200$  km) contraction and (d) 40 Myr ( $\Delta x = 300$  km) contraction. (b and c) Zoomed extracts from Figure 6d showing the small-scale deformation patterns in the foreland fold-and-thrust belts.

extension and subsequent inversion resulting in the uplift of a mildly asymmetric keystone structure. The main characteristics of the third phase are similar to the reference model, with an outward propagating basement thrust sequence building up the pro-wedge. However, both the thin-skinned and thick-skinned thrust sheets forming after the onset of sedimentation are significantly longer than those in the reference model (see Figures 6b and 6c). Upon the onset of deposition, a wide and deep foreland basin forms in the footwall of the active basement thrust sheet. In comparison with the reference model without sedimentation, this basement thrust remains active for a longer time and accommodates more displacement, while the subsequent basement thrust forms further out below the foreland (Figure 6a). During the final phase, the initial keystone structure migrates slightly further into the overriding plate compared to the reference model and the basement thrusts forming in the retro-wedge accommodate more displacement, resulting in a more strongly developed retro-wedge and an overall wider orogen (Figure 6d).

### 3.4. Effect of Erosion: Models M5 and M6

Models M5 (Figure 7) and M6 (Figure 8) have the same basic setup as model M4 but include elevation-dependent erosion in addition to deposition. Erosion is active from the model start but it has a negligible effect in the extensional and inversion phases, as high-elevation topography is only present after uplift of the keystone structure. This means that the initial extension and the early inversion phases are practically identical to those of the reference model.

#### 3.4.1. Moderate Erosion Rate: Model M5

When applying a moderate erosion rate combined with deposition (model M5; Figure 7), a wide domain of basement thrust sheets forming in the third phase becomes exposed in the internal part of the orogen. At the same time, the foreland basins are shallower than the ones observed in model M4, resulting in the deposition of thinner sedimentary successions (Figure 7a). Both the thick-skinned and thin-skinned thrust sheets developing in this model are marginally shorter than in model M4, but still significantly longer than in the reference model. The main effect of erosion is that the developing orogen is narrower (see also

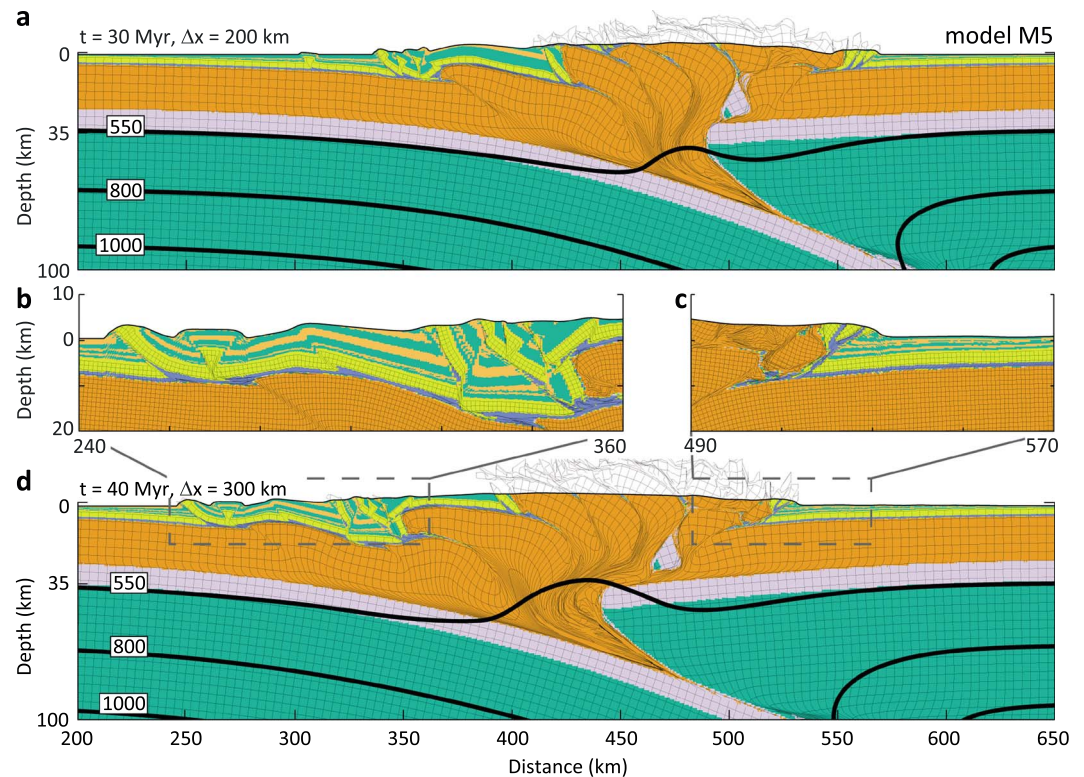


**Figure 7.** Model M5 including simple sedimentation and erosion models. Sedimentation is accounted for with the same algorithm as in model M4. Erosion is modeled using a simple elevation-dependent algorithm. We have scaled the erosion rate so that a 4 km high topography would erode 1 km in 2 Myr. Presenting the same model properties as in the reference model (Figure 2) after (a) 30 Myr ( $\Delta x = 200$  km) contraction and (d) 40 Myr ( $\Delta x = 300$  km) contraction. (b and c) Zoomed extracts from Figure 7d showing the small-scale deformation patterns in the foreland fold-and-thrust belts.

Figure 9). The initial keystone structure migrates more rapidly into the overriding plate and thick-skinned basement deformation in the retro-wedge starts 3 Myr earlier than in the reference model. Despite a significant amount of erosion of the retro-wedge, the lower crustal root of the initial keystone structure is brought only slightly closer to the surface (Figure 7d) in comparison to the previous models.

### 3.4.2. High Erosion Rate: Model M6

In case of more efficient erosion (model M6), the surface exposure of basement structures is more extensive, and the orogen is narrower than in model M5 with moderate erosion (Figures 8 and 9). The initial keystone structure is almost completely removed by erosion and, as a result, the retro-wedge is extremely narrow with all displacement focused along the inverted normal fault. The lower crustal root of the keystone structure has been translated up the inverted normal fault ramp, thrust over the weak décollement layer, and exposed at the surface, sliced in between two basement units at a very external position. The load of the retro-wedge is significantly less than in the previous models, resulting in a shallow retro-foreland basin with little thin-skinned deformation. Moreover, there is no basement deformation penetrating the overriding plate, resulting in the absence of the fourth phase described in the previous models.

## 4. Discussion

### 4.1. Assumptions and Limitations

The aim in this paper is to explore the effects of extensional inheritance and surface processes on the development of doubly vergent orogens. Nevertheless, there are a number of other parameters that exert a significant control on the structural development of such orogens.

One such parameter is the strength of the crust. We have chosen a strong lower crust in our models because it allows for coupling to the frictional-plastic upper mantle lithosphere, resulting in lower crustal

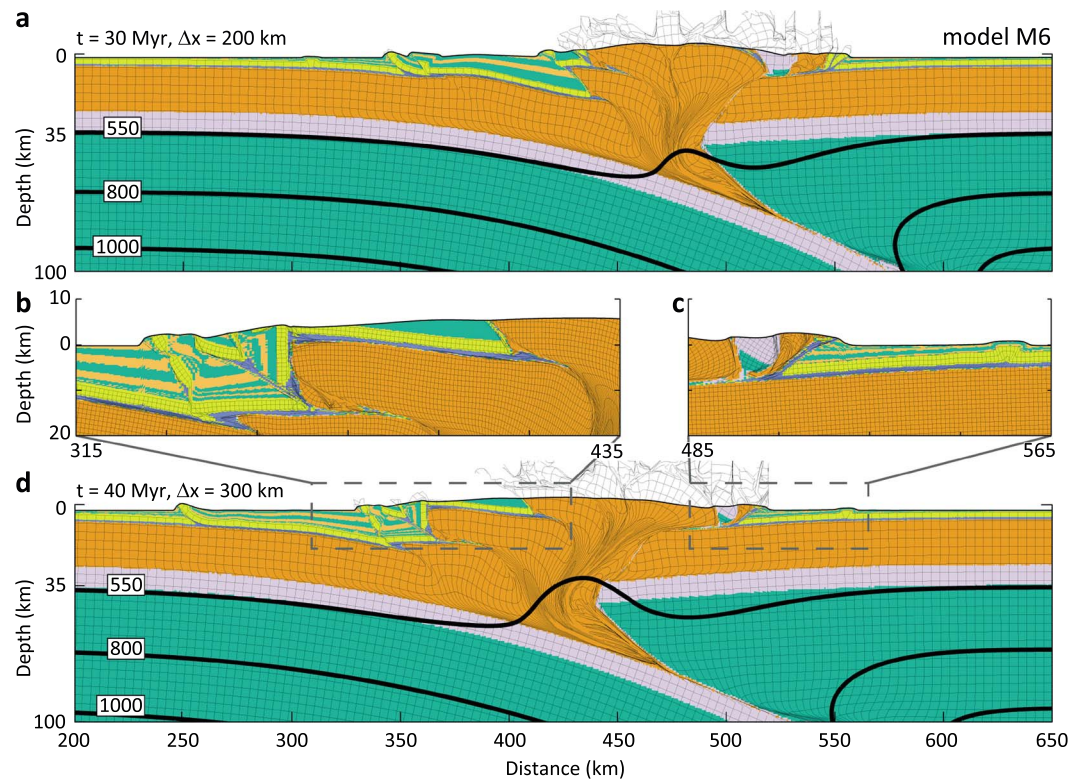


**Figure 8.** Model M6 allowing for simple sedimentation and enhanced erosion processes. Sedimentation and erosion are accounted for using the same algorithms as in model M5, but we have scaled the erosion rate so that in this model a 4 km high topography would erode 1 km in 1 Myr. Presenting the same model properties as in the reference model (Figure 2) after (a) 30 Myr ( $\Delta x = 200$  km) contraction and (d) 40 Myr ( $\Delta x = 300$  km) contraction. (b and c) Zoomed extracts from Figure 8d showing the small-scale deformation patterns in the foreland fold-and-thrust belts.

subduction as observed in many orogens, such as the Pyrenees [e.g., *Etude Continentale et Océanique par Reflexion et Refraction Sismique (ECORS) Pyrenees Team*, 1988; Muñoz, 1992], the Himalaya [Schulte-Pelkum et al., 2005; Nábelek et al., 2009], or the Central Alps [e.g., Schmid et al., 1996]. A weak lower crust could potentially result in a significantly different deformation style at depth and a reduced ability of the crust to support topography.

Another parameter that has a potentially significant bearing on the structural development of the presented accordion models is the length of the postrift thermal relaxation period. By inverting the velocity boundary conditions directly after the rifting phase we have minimized the effect of postrift thermal relaxation. Allowing the rifted lithosphere to cool before the onset of shortening is expected to result in a deeper brittle-ductile transition, and an overall strengthening effect on the extended area. Buitter et al. [2009] showed that thermal relaxation renders basin inversion more difficult, although this effect is counteracted by strain weakening and erosion. Here we have not explored the effect of thermal relaxation on subsequent orogenesis and its consequences remain to be evaluated.

A third model characteristic that we have to keep in mind when interpreting the results is that we added a prerift sediment layer to the models rather than modeling synrift to early postrift sedimentation. This choice is the result of current model limitations. The applied sedimentation model allows only for filling the available accommodation space up to a given reference level, with no upper limit on the amount of material available for deposition. The application of this deposition model during the rifting stage of the model would result in an unreasonable rift geometry with an unrealistically thick (i.e., over 20 km) sedimentary basin. We avoid this by starting sedimentation after the formation of significant positive topography. However, the lack of synrift and postrift sedimentation implies that we cannot explore their potential effects, such as thermal blanketing.

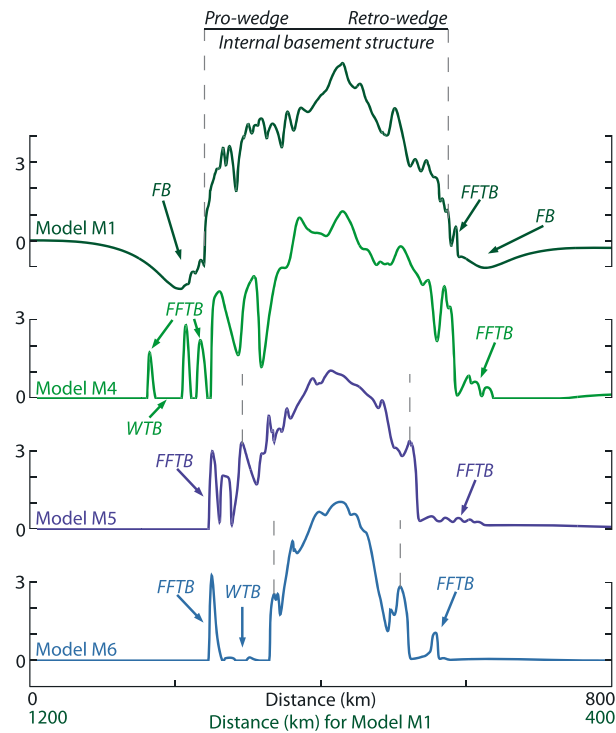


**Figure 9.** Topographic profiles from top to bottom for model M1, model M4, model M5, and model M6, after 40 Myr ( $\Delta x = 300$  km). Key: FB: foreland basin; FFTB: foreland fold-and-thrust belt; WTB: wedge-top basin. The vertical dashed lines indicate the surface traces of the most external basement thrust sheets.

Finally, it is worth pointing out that the initial geometry of the models (e.g., the exact size and position of the weak seed, the thickness of the crust and the relative thicknesses of the upper and lower crust, and position of crustal weak zones) have a controlling effect on the model development.

#### 4.2. The Effects of Extensional Inheritance

The main observed difference between the purely contractional model M2 and the models incorporating explicitly modeled extensional inheritance is provided by the development and structure of the initial keystone structure and the retro-wedge. In the contractional model, the keystone structure constitutes the bulk of the small, undeveloped retro-wedge throughout the model evolution. It has no internal structure and is more or less stationary at the tip of the overriding plate, with the retro-shear zone accommodating very little displacement after the initiation of subduction. The overriding plate remains largely undeformed at all times, with only minor thin-skinned deformation connected to the retro-shear zone (Figure 4). In contrast to the pure contractional case,

models including extensional inheritance show pronounced retro-wedge deformation. After initial inversion and buildup of the orogenic wedge, deformation propagates into the overriding plate. The keystone structure that develops during the inversion of models with extensional inheritance (accordion models) is significantly larger than in the purely contractional case and involves a significant lower crustal and mantle lithospheric root. The main factors that control the degree of retro-wedge deformation are (1) the preexistence of strain-weakened frictional-plastic shear zones that allow reactivation and promote transport of the keystone structure onto the overriding plate and (2) the loading of the retro-wedge mantle lithosphere by the inverted keystone structure, providing access for thickened pro-wedge crust to be translated to the retro-side of the orogen. Thermal relaxation of the growing and thickening crustal-scale orogenic wedge enhances decoupling between the subducting lower crust and the upper crust, thereby further facilitating thrusting of pro-wedge crust onto the retro-wedge. Following initial translation of the keystone structure onto the retro-wedge, further shortening of the retro-wedge crust allows for the development of new thick-skinned thrust sheets in the previously undeformed basement of the overriding plate (Figure 2f) and the formation of a thin-skinned thrust belt on top. Model M3, which extends until full crustal breakup before inversion, exhibits a more complex keystone structure as it includes several inverted normal faults (Figures 3b and 5). However, this does not affect the overall model evolution significantly. Translation of the keystone structure onto the overriding plate is slower; hence, the first basement thrust sheets in the overriding plate form 5 Myr (and 50 km convergence) later, but the general structure is very similar to that of the reference model (compare Figures 2f and 5f). We therefore conclude that the amount of extension experienced by the crust beyond breakup of the rigid lower crust does not strongly affect the overall deformation style in our models.

Additionally, an interesting aspect of our accordion models is that they generate self-consistent inherited weakness zones during extension (e.g., Figure 3), and these weakness zones are preferentially used during

the initial phases of inversion. They exert a first-order control on where and how subduction initiates. The initial rifted basin developing during extension is generally very slightly asymmetric by the end of the 50 Myr extensional phase. This asymmetry becomes more evident with the increased amount of extension in model M3. The polarity of the following subduction correlates perfectly with the direction of this asymmetry (see the supporting information) pointing to the controlling nature of the inherited extensional weakness zones. The earlier models of *Jammes and Huismans* [2012] did not have sufficient resolution to resolve this.

#### 4.3. The Effects of Synorogenic Sedimentation

The effects of sedimentation on the evolution of an inverted rift basin can be best understood by comparing the reference models M1 (Figure 2) and M4 (Figure 6). Syntectonic sedimentation leads to the development of a wide and deep sedimentary fold-and-thrust belt in the foreland depression in front of the pro-wedge. As a result of sediment loading, the active frontal basement thrust remains active for a longer time and accommodates more displacement, while the subsequent new basement thrust forms farther out below the foreland. In the presence of extensional inheritance (model M4; Figure 6) the additional mass of the initial keystone structure loading the overriding plate is sufficient to create a deep foreland depression that can accommodate a significant amount of synorogenic sediments. Sedimentation also significantly affects thin-skinned deformation on both sides of the orogen, creating complex sets of long thrust sheets and pop-up structures, with generally more displacement along the base of the individual units than observed in the reference model (Figures 6b and 6c).

Concerning the thin-skinned deformation of sedimentary fold-and-thrust belts, our model results are in good agreement with recent modeling results of *Fillon et al.* [2012], who demonstrated a strong correlation between thin-skinned thrust sheet length and the thickness of synorogenic sediments loading the foreland fold-and-thrust belt.

#### 4.4. The Effects of Erosion

The effects of erosion on orogenic evolution in the presence of extensional inheritance can be best understood by comparing models M4, M5, and M6 (Figures 6–8; see also Figure 9). Erosion facilitates the localization of deformation by reducing the load (and therefore the gravitational stresses) in the core of the orogenic wedge, thus leading to a decrease in wedge width [e.g., *Willett*, 1999]. Moreover, simple mass budget considerations also require that the wedge width decreases with increasing erosion rate, all else remaining equal [*Dahlen*, 1990; *Whipple and Meade*, 2004]. In the model with a moderate erosion rate (model M5), basement is extensively exposed in the central part of the orogen. As the internal mass of the orogen is reduced by erosion, orogenic loading becomes less effective in creating foreland depressions. As a result, the foreland fold-and-thrust belts are thinner and less developed than the ones observed in model M4 that does not include erosion (Figure 6). Reduced synorogenic loading in turn limits the effect of sedimentation on basement structure. Even with moderate amounts of deposition, the elongation of both the thick-skinned and the thin-skinned thrust sheets is still apparent. Higher erosion rates enhance localization of deformation into a very narrow orogenic wedge (Figure 9), preventing the migration of deformation into the undeformed basement of the overriding plate and resulting in a less developed retro-wedge (e.g., model M6; Figure 8).

#### 4.5. Interaction of Thin-Skinned and Thick-Skinned Tectonics

The pre-tectonic sediments, including a weak basal décollement horizon, allow for investigating the interaction between thin-skinned and thick-skinned tectonic styles. Both the accordion and the pure contractional models show that the thin-skinned thrust sheets are generally rooted in the footwall of new basement thrusts that are formed in an outward propagating sequence (e.g., model M1; Figures 2d and 2e). Following the formation of a new basement thrust, the earlier, more proximal thin-skinned deformation is abandoned and a new thin-skinned thrust is activated in front of the basement thrust sheet. In contrast, thin-skinned thrusts forming ahead of basement deformation in the foreland do not affect the position of a new basement thrust below the foreland. Thus, it is the thick-skinned basement deformation that drives thin-skinned deformation in the sedimentary cover, the coupling in the opposite sense being significantly less efficient.

In the absence of syntectonic sedimentation (e.g., model M1; Figures 2d and 2e) the individual thin-skinned thrust sheets have very similar length scale and their regular activation in an “accretion cycle” [e.g., *Hoth et al.*, 2007] can be understood from minimum-work principles [*Hardy et al.*, 1998; *Masek and Duncan*, 1998]. When syntectonic sedimentation is included (e.g., model M4; Figures 6b and 6c), the thin-skinned thrust

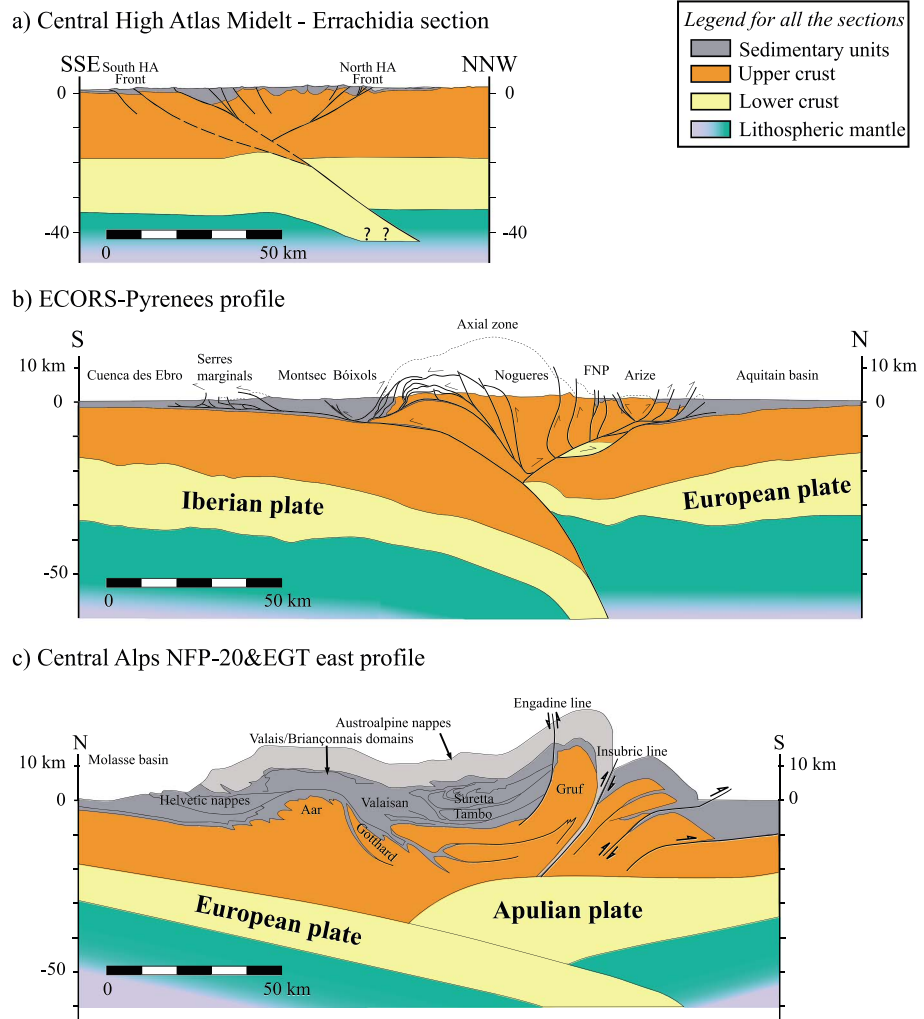


**Figure 10.** Natural examples. Crustal-scale cross sections from (a) the Central High Atlas redrawn after *Arboleya et al.* [2004] and *Ayarza et al.* [2005], (b) the Central Pyrenees after *Muñoz* [1992] and *Beaumont et al.* [2000], and (c) the European Central Alps after *Schmid and Kissling* [2000].

sheets forming in the foreland fold-and-thrust belts become significantly longer. Basement deformation and sediment loading interact in forcing both the thin- and thick-skinned fold-and-thrust belt structure. While sediment loading results in longer thin- and thick-skinned thrust sheets, basement deformation triggers thin-skinned thrust formation where the basement shear zones reach the basal décollement. As a result, the thin-skinned thrust sheets observed in the models with syntectonic sedimentation display different length scales. The introduction of erosion in the models does not affect the general behavior of the thin-skinned fold-and-thrust belts forming in the forelands, as most erosion takes place in the internal parts of the orogen. Both the preorogenic and synorogenic sediments are gradually eroded from these models, leaving a growing area of basement rocks exposed in the orogenic core.

### 5. Comparison With Natural Systems

The lithosphere-scale thermo-mechanical models presented here demonstrate the fundamental influence of lithospheric strength, extensional inheritance, and surface processes on the structural evolution of mountain belts. In the following sections we will summarize the first-order structure of three orogens formed by inversion of a prior rift or rifted passive margin displaying different deformation styles: the High Atlas, the Pyrenees, and the Central Alps. We will compare these observations to our results in order to assess how we could explain the observed differences in the framework of our models.



### 5.1. The High Atlas

The Moroccan High Atlas Mountains provide a good example of an intracontinental mountain belt [Rogers, 1987; Ziegler *et al.*, 1995] and formed during Cenozoic times within the interior of the African plate, due to compression resulting from the convergence between Africa and Europe [Teixell *et al.*, 2003]. The chain developed from the inversion of Jurassic rift and transtensional basins and is made up of Mesozoic sediments deposited in these basins, with minor pre-Mesozoic and Cenozoic occurrences [Arboleya *et al.*, 2004, and references therein]. Pre-Mesozoic Hercynian basement rocks are only exposed at the surface in eroded antiforms. The High Atlas, similar to other intracontinental mountain belts, experienced moderate crustal shortening, yet it has very high topography, with peaks over 4000 m [Teixell *et al.*, 2003]. The anomalous topography is commonly associated with a mantle contribution to the uplift [e.g., Teixell *et al.*, 2003; Missenard *et al.*, 2006]. In the central part of the orogen, most of the Alpine deformation is accommodated in a 100 km wide belt (Figure 10a after Arboleya *et al.* [2004] and Ayarza *et al.* [2005]). Deformation is mostly restricted to the upper crust, while the approximately 13–15 km thick lower crust underthrusts the overriding plate with the mantle lithosphere [Wigger *et al.*, 1992; Ayarza *et al.*, 2005]. The estimated total shortening along this section is in the order of 30 km [Teixell *et al.*, 2003].

Most of the contractional deformation is accommodated along the North and South High Atlas fronts, with minor thin-skinned folding in the forelands and a number of crustal-scale, thick-skinned inverted extensional structures present in between (Figures 10a). Synorogenic erosion and sedimentation is very limited across the belt. These characteristics are to first order consistent with the early inversion stage of Model M1 (Figure 2b). The North and South High Atlas fronts can be seen as analogues for the shear zones on either side of the keystone structure in our accordion models, with no major inverted normal faults observed at more distal positions from the orogen.

### 5.2. The Pyrenees

The Pyrenees (Figure 10b) are a collisional orogen formed between the Late Cretaceous (90 Ma) and Early Miocene (20 Ma) as a result of convergence between the Iberian and European plates [Roest and Srivastava, 1991; Rosenbaum *et al.*, 2002; Vissers and Meijer, 2012]. The range is dominated by inversion tectonics [Muñoz *et al.*, 1986], owing to thrusting along inherited extensional structures that were originally formed during Triassic to Cretaceous rifting and transtension, associated with anticlockwise rotation of the Iberian plate with respect to Europe [Roest and Srivastava, 1991; Rosenbaum *et al.*, 2002]. Here we focus on the Central Pyrenean Etude Continentale et Océanique par Reflexion et Refraction Sismique seismic section [ECORS Pyrenees Team, 1988] and the associated balanced section restoration [Muñoz, 1992].

Underthrusting of the Iberian crust below the European crust results in an asymmetric wedge, featuring a wide southern pro-wedge and a narrower northern retro-wedge. In the center of the belt, the Axial Zone comprises a south vergent antiformal stack of upper crustal thrust sheets [Muñoz, 1992]. The Axial Zone is flanked toward the south by the South Pyrenean Unit, a fold-and-thrust belt consisting of Mesozoic and Cenozoic sedimentary rocks. North of the Axial Zone, in the North Pyrenean Unit, basement and cover rocks form steep, north vergent thrust sheets, and pop-up structures [Muñoz, 1992; Capote *et al.*, 2002].

The presence of a dense, presumably lower crustal, body preserved at shallow depth below the North Pyrenean Unit as inferred from gravity data [Torné *et al.*, 1989], together with the inverted extensional structures of the retro-wedge, are features that can only be observed in and explained by our accordion models and are a direct result of extensional inheritance. Moreover, the active imbrication of thick-skinned thrust sheets with a wide thin-skinned foreland fold-and-thrust belt in the pro-wedge, coupled with the relatively slow retro-wedge deformation and shallower retro-foreland basin, can all be observed at the intermediate stage of development in the accordion models of M1 and M5 (Figures 2c and 7a). The widespread exposure of basement structures in the axial zone is well reproduced by model M5, including moderate erosion (Figure 7a). The estimated 160 km of shortening [Beaumont *et al.*, 2000] is also consistent with the modeled amount of contraction at these intermediate model stages.

### 5.3. The Central Alps

The European Alps record the closure of the Tethys ocean basins (Piémont-Ligurian Ocean) during convergence of the African and European plates [Stampfli *et al.*, 2001]. The crustal structure is well constrained by several crustal-scale deep seismic transects crossing the Alps. Although these sections show

significant along strike variation, some first-order crustal-scale features are observed in all of them. These common features are (1) east-south-east to south directed subduction of the European lithosphere, (2) a seismic gap between the European and Adriatic (or Apulian) Moho, and (3) strong decoupling between upper and lower crust, with the lower crust underthrusting along with the mantle lithosphere and upper crustal shortening resulting in the main body of the orogen [Schmid *et al.*, 1996; Schmid and Kissling, 2000; Schmid *et al.*, 2004]. Here we focus on the profile crossing the Central Alps, NFP-20 EAST&EGT (Figure 10c) [after Schmid and Kissling, 2000]. Note that both extension and convergence in the Alps have progressed significantly further than in the other two examples, i.e., several hundred kilometers of oceanic lithosphere have been subducted below the Alps and orogenic shortening is estimated at ~300 km [Schmid *et al.*, 1996; Stampfli *et al.*, 2001].

The most dominant features of the internal part of this section is the stacking of crustal-scale thrusts derived from the European margin (i.e., Helvetic and Briançonnais units) under the Penninic nappes (Figure 10c). This complex structure is reproduced to first order in our model M5 (Figure 7d), along with the Insubric back thrust and to a lesser extent the development of the Austroalpine nappes. The 300 km of shortening estimated for this section after the subduction of the Piemont-Ligurian Ocean [Schmid *et al.*, 1996, Table 1] is consistent with the amount of contraction at this stage of model development. It has to be noted, however, that due to the incorporation of an oceanic domain the materials accreted in the orogen are much more heterogeneous than in our models, leading to richer structural styles such as recumbent fold nappes and out-of-sequence thrusting. Some of the complexities introduced by the extensional inheritance and the strike slip deformation accommodated along the Insubric line, along with the significant erosion of the internal part of the orogen can explain the existence of lithospheric mantle fragments at shallow depths.

## 6. Conclusions

In this study we have used thermo-mechanical model experiments to explore the effects of surface processes and extensional inheritance on the structural evolution of contractional orogens and their foreland basins. Bearing in mind the model limitations, we draw the following conclusions:

1. Extensional inheritance plays a fundamental role, facilitating the migration of deformation into the undeformed basement of the overriding plate. Moreover, a significant amount of lower crustal/mantle-lithospheric material is preserved at shallow depths in the presence of extensional inheritance but high erosion rates are needed to bring this material to the surface.
2. The amount of extension experienced by the crust beyond breakup of the rigid lower crust until full crustal breakup does not affect the overall deformation style strongly. An initial keystone structure that later delimits the retro-wedge becomes somewhat larger and more complex when extension is allowed to run to full crustal breakup, but the general features remain largely unaffected.
3. In case of the accordion models, the asymmetry of the extensional structures developed during the initial rifting phase controls the polarity of the subduction during the subsequent contraction.
4. Sedimentation results in longer basement thrust sheets as well as longer thin-skinned thrust sheets and a generally wider orogenic belt. The active frontal basement thrust remains active for a longer time, accommodating more displacement, while subsequent basement thrusts form further out below the foreland, creating longer thrust sheets. In the presence of inherited extensional structures this is also true in the retro-wedge, even though the thrust sheets developing there are consistently shorter than those developing in the pro-wedge.
5. In the presence of preorogenic and/or synorogenic sediments, thin-skinned fold-and-thrust belts form above the basement thrust sheets. The thin-skinned thrust sheets are generally rooted in the footwall of the basement thrusts as they form in an outward propagating sequence. Following the formation of a new basement thrust, the earlier, more proximal thin-skinned deformation sequence is abandoned in favor of a new thin-skinned thrust forming in front of the new basement thrust sheet. In contrast, the thin-skinned thrusts forming ahead of the basement deformation structures in the foreland do not affect the position of a new basement thrust.
6. Erosion removes material from the internal part of the orogen, narrowing the wedge and reducing the orogenic load on the colliding plates, hence limiting the space available for deposition in the foreland basins and thereby limiting the effects of sedimentation on foreland structures described above.

High erosion rates also enhance localization of deformation into a narrow orogenic wedge, preventing its migration into the undeformed basement of the overriding plate.

7. The crustal structure at different stages of the accordion models presented in this study show good first-order correlation with structural features observed in the High Atlas, the Central Pyrenees, and the Central Alps.

#### Acknowledgments

This study is supported by the Norwegian Research Council that funded the Norwegian component of the European Science Foundation Eurocore TOPO-Europe project PyrTec. The Bergen Center of Computational Science is acknowledged for access to computational infrastructure. Parameter values used to produce the numerical model results are provided in Table 1. We thank Laetitia Le Pourhiet and Kosuke Ueda for their detailed and insightful comments on the manuscript.

#### References

- Arboleya, M. L., A. Teixell, M. Charroud, and M. Julivert (2004), A structural transect through the High and Middle Atlas of Morocco, *J. Afr. Earth Sci.*, 39(3–5), 319–327, doi:10.1016/j.jafrearsci.2004.07.036.
- Avouac, J. P., and E. B. Burov (1996), Erosion as a driving mechanism of intracontinental mountain growth, *J. Geophys. Res.*, 101(B8), 17,747–17,769, doi:10.1029/96JB01344.
- Ayarza, P., F. Alvarez-Lobato, A. Teixell, M. L. Arboleya, E. Teson, M. Julivert, and M. Charroud (2005), Crustal structure under the central High Atlas Mountains (Morocco) from geological and gravity data, *Tectonophysics*, 400(1–4), 67–84, doi:10.1016/j.tecto.2005.02.009.
- Bassi, G., C. E. Keen, and P. Potter (1993), Contrasting styles of rifting: Models and examples from the Eastern Canadian Margin, *Tectonics*, 12, 639–655, doi:10.1029/93TC00197.
- Beaumont, C., P. Fullsack, and J. Hamilton (1992), Erosional control of active compressional orogens, in *Thrust Tectonics*, edited by K. R. McClay, pp. 1–18, Chapman and Hall, London.
- Beaumont, C., P. Fullsack, and J. Hamilton (1994), Styles of crustal deformation in compressional orogens caused by subduction of the underlying lithosphere, *Tectonophysics*, 232(1–4), 119–132, doi:10.1016/0040-1951(94)90079-5.
- Beaumont, C., J. A. Muñoz, J. Hamilton, and P. Fullsack (2000), Factors controlling the Alpine evolution of the central Pyrenees inferred from a comparison of observations and geodynamical models, *J. Geophys. Res.*, 105(B4), 8121–8145, doi:10.1029/1999JB900390.
- Bonnet, C., J. Malavieille, and J. Mosar (2007), Interactions between tectonics, erosion, and sedimentation during the recent evolution of the Alpine orogen: Analogue modeling insights, *Tectonics*, 26, TC6016, doi:10.1029/2006TC002048.
- Bos, B., and C. J. Spiers (2002), Frictional-viscous flow of phyllosilicate-bearing fault rock: Microphysical model and implications for crustal strength profiles, *J. Geophys. Res.*, 107(B2), 2028, doi:10.1029/2001JB000301.
- Buck, W. R. (1991), Modes of continental lithospheric extension, *J. Geophys. Res.*, 96(B12), 20,161–20,178, doi:10.1029/91JB01485.
- Buck, W. R., L. L. Lavier, and A. Poliakov (1999), How to make a rift wide, *Philos. Trans. R. Soc. London, Ser. A*, 357(1753), 671–693, doi:10.1098/rsta.1999.0348.
- Buiter, S. J. H. (2012), A review of brittle compressional wedge models, *Tectonophysics*, 530–531, 1–17, doi:10.1016/j.tecto.2011.12.018.
- Buiter, S. J. H., and O. A. Pfiffner (2003), Numerical models of the inversion of half-graben basins, *Tectonics*, 22(5), 1057, doi:10.1029/2002TC001417.
- Buiter, S. J. H., O. A. Pfiffner, and C. Beaumont (2009), Inversion of extensional sedimentary basins: A numerical evaluation of the localisation of shortening, *Earth Planet. Sci. Lett.*, 288(3–4), 492–504, doi:10.1016/j.epsl.2009.10.011.
- Capote, R., J. A. Muñoz, J. L. Simon, C. L. Liesa, and L. E. Arlegui (2002), Alpine tectonics I: The Alpine system north of the Betic Cordillera, in *The Geology of Spain*, edited by W. Gibbon and T. Moreno, pp. 367–400, Geol. Soc. London, London.
- Chapple, W. M. (1978), Mechanics of thin-skinned fold-and-thrust belts, *Geol. Soc. Am. Bull.*, 89, 1189–1198.
- Dahlen, F. A. (1990), Critical taper model of fold-and-thrust belts and accretionary wedges, *Annu. Rev. Earth Planet. Sci.*, 18, 55–99, doi:10.1146/annurev.earth.18.1.55.
- DeCelles, P. G., and K. A. Giles (1996), Foreland basin systems, *Basin Res.*, 8(2), 105–123, doi:10.1046/j.1365-2117.1996.01491.x.
- Etude Continentale et Océanique par Reflexion et Refraction Sismique (ECORS) Pyrenees Team (1988), The ECORS deep reflection seismic survey across the Pyrenees, *Nature*, 331, 508–511.
- Ellis, S., C. Beaumont, R. A. Jamieson, and G. Quinlan (1998), Continental collision including a weak zone: The vise model and its application to the Newfoundland Appalachians, *Can. J. Earth Sci.*, 35(11), 1323–1346, doi:10.1139/E97-100.
- Fillon, C., R. S. Huismans, and P. van der Beek (2012), Syntectonic sedimentation effects on the growth of fold-and-thrust belts, *Geology*, 41(1), 83–86, doi:10.1130/g33531.1.
- Ford, M. (2004), Depositional wedge tops: Interaction between low basal friction external orogenic wedges and flexural foreland basins, *Basin Res.*, 16(3), 361–375, doi:10.1111/j.1365-2117.2004.00236.x.
- Gleason, G. C., and J. Tullis (1995), A flow law for dislocation creep of quartz aggregates determined with the molten-salt cell, *Tectonophysics*, 247(1–4), 1–23, doi:10.1016/0040-1951(95)00011-B.
- Hardy, S., C. Duncan, J. Masek, and D. Brown (1998), Minimum work, fault activity and the growth of critical wedges in fold and thrust belts, *Basin Res.*, 10(3), 365–373, doi:10.1046/j.1365-2117.1998.00073.x.
- Hoth, S., A. Hoffmann-Rothe, and N. Kukowski (2007), Frontal accretion: An internal clock for bivergent wedge deformation and surface uplift, *J. Geophys. Res.*, 112, B06408, doi:10.1029/2006JB004357.
- Huismans, R. S., and C. Beaumont (2003), Symmetric and asymmetric lithospheric extension: Relative effects of frictional-plastic and viscous strain softening, *J. Geophys. Res.*, 108(B10), 2496, doi:10.1029/2002JB002026.
- Huismans, R. S., and C. Beaumont (2011), Depth-dependent extension, two-stage breakup and cratonic underplating at rifted margins, *Nature*, 473(7345), 74–78, doi:10.1038/nature09988.
- Huismans, R. S., S. J. H. Buiter, and C. Beaumont (2005), Effect of plastic-viscous layering and strain softening on mode selection during lithospheric extension, *J. Geophys. Res.*, 110, B02406, doi:10.1029/2004JB003114.
- Jamieson, R. A., and C. Beaumont (2013), On the origin of orogens, *Geol. Soc. Am. Bull.*, 125(11–12), 1671–1702, doi:10.1130/B30855.1.
- Jammes, S., and R. S. Huismans (2012), Structural styles of mountain building: Controls of lithospheric rheologic stratification and extensional inheritance, *J. Geophys. Res.*, 117, B10403, doi:10.1029/2012JB009376.
- Karato, S., and P. Wu (1993), Rheology of the upper mantle: A synthesis, *Science*, 260(5109), 771–778, doi:10.1126/science.260.5109.771.
- Lavier, L. L., R. W. Buck, and A. Poliakov (2000), Factors controlling normal fault offset in an ideal brittle layer, *J. Geophys. Res.*, 105, 23,431–23,442, doi:10.1029/2000JB900108.
- Masek, J. G., and C. C. Duncan (1998), Minimum-work mountain building, *J. Geophys. Res.*, 103(B1), 907–917, doi:10.1029/97JB03213.
- Missenard, Y., H. Zeyen, D. Frizon de Lamotte, P. Leturmy, C. Petit, M. Sébrier, and O. Saddiqi (2006), Crustal versus asthenospheric origin of relief of the Atlas Mountains of Morocco, *J. Geophys. Res.*, 111, B03401, doi:10.1029/2005JB003708.
- Mouthereau, F., J. Tensi, N. Bellahsen, O. Lacombe, T. De Boisgrollier, and S. Kargar (2007), Tertiary sequence of deformation in a thin-skinned/thick-skinned collision belt: The Zagros Folded Belt (Fars, Iran), *Tectonics*, 26, TC5006, doi:10.1029/2007TC002098.

- Mouthereau, F., A. B. Watts, and E. Burov (2013), Structure of orogenic belts controlled by lithosphere age, *Nat. Geosci.*, 6(9), 785–789, doi:10.1038/ngeo1902.
- Mugnier, J. L., P. Baby, B. Colletta, P. Vinour, P. Bale, and P. Leturmy (1997), Thrust geometry controlled by erosion and sedimentation: A view from analogue models, *Geology*, 25(5), 427–430, doi:10.1130/0091-7613(1997)025<0427:Tgcbca>2.3.Co;2.
- Muñoz, J. A. (1992), Evolution of a continental collision belt: ECORS Pyrenees crustal balanced cross section, in *Thrust Tectonics*, edited by K. R. McClay, pp. 235–246, Chapman and Hall, New York.
- Muñoz, J. A., A. Martínez, and J. Verges (1986), Thrust sequences in the Eastern Spanish Pyrenees, *J. Struct. Geol.*, 8(3–4), 399–405, doi:10.1016/0191-8141(86)90058-1.
- Nábelek, J., G. Hetényi, J. Vergne, S. Sapkota, B. Kafle, M. Jiang, H. Su, J. Chen, B.-S. Huang, and the HI-CLIMB Team (2009), Underplating in the Himalaya-Tibet collision zone revealed by the HI-CLIMB experiment, *Science*, 325, 1371–1374, doi:10.1126/science.1167719.
- Rodgers, J. (1987), Chains of basement uplifts within cratons marginal to orogenic belts, *Am. J. Sci.*, 287(7), 661–692.
- Roest, W. R., and S. P. Srivastava (1991), Kinematics of the plate boundaries between Eurasia, Iberia, and Africa in the North-Atlantic from the Late Cretaceous to the present, *Geology*, 19(6), 613–616, doi:10.1130/0091-7613(1991)019<0613:Kotpb>2.3.Co;2.
- Rosenbaum, G., G. S. Lister, and C. Duboz (2002), Relative motions of Africa, Iberia and Europe during Alpine orogeny, *Tectonophysics*, 359(1–2), 117–129, doi:10.1016/S0040-1951(02)00442-0.
- Schmid, S. M., and E. Kissling (2000), The arc of the western Alps in the light of geophysical data on deep crustal structure, *Tectonics*, 19(1), 62–85, doi:10.1029/1999TC900057.
- Schmid, S. M., O. A. Pfiffner, N. Froitzheim, G. Schonborn, and E. Kissling (1996), Geophysical-geological transect and tectonic evolution of the Swiss-Italian Alps, *Tectonics*, 15(5), 1036–1064, doi:10.1029/96TC00433.
- Schmid, S. M., B. Fügenschuh, E. Kissling, and R. Schuster (2004), Tectonic map and overall architecture of the Alpine orogen, *Eclogae Geol. Helv.*, 97(1), 93–117, doi:10.1007/s00015-004-1113-x.
- Schulte-Pelkum, V., G. Monsalve, A. Sheehan, M. R. Pandey, S. Sapkota, R. Bilham, and F. Wu (2005), Imaging the Indian subcontinent beneath the Himalaya, *Nature*, 435, 1222–1225.
- Sibson, R. H. (1990), Conditions for fault-valve behaviour, *Geol. Soc. Spec. Publ.*, 54, 15–28.
- Simpson, G. D. H. (2006), Modelling interactions between fold-thrust belt deformation, foreland flexure and surface mass transport, *Basin Res.*, 18(2), 125–143, doi:10.1111/j.1365-2117.2006.00287.x.
- Stampfli, G., J. Mosar, P. Favre, A. Pillevert, and J. C. Vannay (2001), Permo-Mesozoic evolution of the western Tethys realm: The Neo-Tethys East Mediterranean Basin connection, in *Peri-Tethys Memoir 6: Peri-Tethyan Rift/Wrench Basins and Passive Margins*, edited by P. A. Ziegler, pp. 51–108, *Mém. Mus. Natn. Hist. Nat.*, Paris.
- Stolar, D. B., S. D. Willett, and G. H. Roe (2006), Climatic and tectonic forcing of a critical orogen, *Geol. Soc. Am. Spec. Pap.*, 398, 241–250, doi:10.1130/2006.2398(14).
- Storti, F., and K. McClay (1995), Influence of syntectonic sedimentation on thrust wedges in analog models, *Geology*, 23(11), 999–1002, doi:10.1130/0091-7613(1995)023<0999:lossot>2.3.Co;2.
- Streit, J. E. (1997), Low frictional strength of upper crustal faults: A model, *J. Geophys. Res.*, 102(B11), 24,619–24,626, doi:10.1029/97JB01509.
- Teixell, A., M.-L. Arboleya, M. Julivert, and M. Charroud (2003), Tectonic shortening and topography in the central High Atlas (Morocco), *Tectonics*, 22(5), 1051, doi:10.1029/2002TC001460.
- Thieulot, C. (2011), FANTOM: Two- and three-dimensional numerical modelling of creeping flows for the solution of geological problems, *Phys. Earth Planet. Inter.*, 188(1–2), 47–68, doi:10.1016/j.pepi.2011.06.011.
- Torné, M., B. Decabissole, R. Bayer, A. Casas, M. Daignieres, and A. Rivero (1989), Gravity constraints on the deep-structure of the Pyrenean belt along the ECORS profile, *Tectonophysics*, 165(1–4), 105–116, doi:10.1016/0040-1951(89)90039-5.
- Vissers, R. L. M., and P. T. Meijer (2012), Iberian plate kinematics and Alpine collision in the Pyrenees, *Earth Sci. Rev.*, 114(1–2), 61–83, doi:10.1016/j.earscirev.2012.05.001.
- Whipple, K. X. (2009), The influence of climate on the tectonic evolution of mountain belts, *Nat. Geosci.*, 2(2), 97–104, doi:10.1038/ngeo413.
- Whipple, K. X., and B. J. Meade (2004), Controls on the strength of coupling among climate, erosion, and deformation in two-sided, frictional orogenic wedges at steady state, *J. Geophys. Res.*, 109, F01011, doi:10.1029/2003JF000019.
- Wigger, P., G. Asch, P. Giese, W. D. Heinsohn, S. O. Elalami, and F. Ramdani (1992), Crustal structure along a traverse across the Middle and High Atlas mountains derived from seismic refraction studies, *Geol. Rundsch.*, 81(1), 237–248, doi:10.1007/Bf01764552.
- Willett, S., C. Beaumont, and P. Fullsack (1993), Mechanical model for the tectonics of doubly vergent compressional orogens, *Geology*, 21(4), 371–374, doi:10.1130/0091-7613(1993)021<0371:Mmftto>2.3.Co;2.
- Willett, S. D. (1999), Orogeny and orography: The effects of erosion on the structure of mountain belts, *J. Geophys. Res.*, 104(B12), 28,957–28,981, doi:10.1029/1999JB900248.
- Ziegler, P. A., S. Cloetingh, and J. D. van Wees (1995), Dynamics of intra-plate compressional deformation: The Alpine foreland and other examples, *Tectonophysics*, 252(1–4), 7–59, doi:10.1016/0040-1951(95)00102-6.